Research Article

Field Testing and Numerical Simulation of the Dynamic Response of Loess Hill Site under High–Speed Train Load

Wujian Yan [ID],[1] Xinxin Tian,[1] Ping Wang [ID],[1] Lin Kang,[1] and Zhijian Wu [ID][2]

[1]*Lanzhou Institute of Seismology, Key Laboratory of Loess Earthquake Engineering, China Earthquake Administration, Lanzhou 730000, China*
[2]*College of Transportation Engineering, Nanjing Tech University, Nanjing 211800, China*

Correspondence should be addressed to Zhijian Wu; zhijian@njtech.edu.cn

In this study, the loess hill site of an elevated bridge section in Tongwei-Qin'an of the Baolan high-speed railroad was selected as the research object, and the vibration acceleration of the loess hill site under the elevated bridge was tested in the field under the train operating load. The results show that under the same intensity of train load, the time range of vibration acceleration observed by field test and numerical simulation decays linearly with increasing distance from the source, while the amplification effect appears in the loess hill site at a greater distance, and the vibration duration also appears to increase. The vibration acceleration waveforms at each observation point observed by field tests and numerical simulations are similar, and the peak vertical acceleration at each observation point obtained from numerical simulations is overall greater than the peak acceleration at each point obtained from field tests, with $a_{\text{Simulated}-\max}/a_{\text{Observed}-\max}$ values ranging from 1.04 to 1.63. The Fourier spectrum frequencies recorded by numerical simulation and field test are mainly concentrated in the range of 1~40 Hz, but the difference between the main frequencies recorded by the two is large. The main frequency of the energy spectrum recorded by the numerical simulation is around 15 Hz, which is the same as the main frequency of the energy spectrum vibration of the input vibration wave, and the main frequency of the energy spectrum vibration recorded by the field test is around 25 Hz.

1. Introduction

There are various complex topographical features along the high-speed railroad line, and the dynamic response of different topographical features under the high-speed train load is not the same. In recent years, with the growth of the urban population and people's travelling needs are also getting bigger and bigger, so that the contradiction between the production and life of people and the increasing demand for transport is becoming more and more prominent. On the one hand, due to the factors of safety, economy, and comfort of high-speed train operation, it becomes the primary tool for people to travel; on the other hand, the vibration problem caused by high-speed trains is becoming more and more serious, causing the vibration of buildings along the line and generating a lot of noise, which seriously affects the normal life of residents along the line. In addition, the environmental vibration caused by high-speed trains is closely related to the nature of the soil of the site, the form of the railroad section, the running speed of the train, and the grouping of the train.

During the past decades, many researches have been carried out to unravel the vibration problems. These studies mainly can be divided into three categories: theoretical analysis [1–6], numerical simulation, and field test. However, field test and numerical calculation are the most common and important methods to study vibration. Regarding the numerical simulation, the finite element (FE) numerical simulation is a very effective method to predict and analyze the track-subgrade behavior and the ground vibration induced by train loads. Xia et al. [7] studied the vibration of ground and buildings caused by train operation under elevated bridges through field tests and found that the vibration intensity had a significant relationship with the train speed, and the ground vibration was amplified in a certain range. Gao et al. [8] studied the vibration of the

ground along the Qin-Shen railroad using field testing techniques and discussed the effect of train grouping and speed on vibration. Chen et al. [9] tested and studied the vibration characteristics of the ground in a section of the Beijing–Guangzhou railway and its attenuation law. Guo-yuan et al. [10, 11] analyzed the vibration characteristics and found that the graded gravel section could significantly reduce the settlement based on the vibration and settlement field test results of railroad road bridges and road culverts. Zhang [12] tested the vibration caused by the train operation under the viaduct and analyzed the vibration isolation effect of the barrier. Xiao et al. [13] tested and analyzed the vibration caused by train operation in the tunnel in three directions and found that the vibration in the vertical direction is smaller than that in the circular and radial directions, and there is a vibration amplification zone within a certain distance from the center of the tunnel. Zhang [14] and Gong-qi [15] studied the vibration generated by train operation in the embankment section using field measurements and numerical simulations. Xiang-Lian and Zhou [16] studied the vibration of the site during the passage of trains along the West-Bao railroad through field actual measurements and found that the vibration in each direction of vibration increases with the increase of train speed and axle weight, and there is a vibration amplification in a certain range. Wu et al. [17, 18] studied the vibration characteristics of the permafrost area under train load and the deformation characteristics of the soil under repeated train load and found that the vibration would attenuate substantially when passing through the embankment, and the deformation of the soil would reach the maximum in the first year of train operation and finally stabilize. Wang et al. [19] tested the vibration caused by train operation in different seasons of the roadbed section in the seasonal permafrost area, and found that the vibration of the site in winter is due to the soil is in the frozen state, the modulus of elasticity of the soil increases, and the damping ratio decreases, and the peak vibration acceleration of each component is larger, but in the spring thawing season, the soil contains a large amount of water, which results in the vibration acceleration of the peak of the vibration in all directions is a phenomenon of decreasing. The peak acceleration in the horizontal direction is slightly enhanced. Chen and Zhou [20] established the 3D FEM of the vehicle-track-subgrade coupling systems to study the different stiffness effects of the subgrade surface layer, bottom layer, embankment, foundation, and fastener by analyzing the vertical displacement of the track-subgrade. Connolly et al. [21, 22] established a three-dimensional numerical model to study the vibration characteristics of embankment in the soft soil regions under train loads. Degrande et al. [23] presented a three-dimensional FEM of tunnel soil to predict the vibrations in the free field from excitation. Andersen and Jones [24] compared the 2D and 3D FEM of railway tunnels. These results showed that the 2D soil-tunnel FEM could effectively calculate the dynamic response of soil and tunnels. Lyratzakis et al. [25] established a 3D FEM to analyze the influence of HST-induced vibration on the adjacent buildings and applied the efficient measure to minimize the vibration. Bian et al. [26] calculated the

dynamic response of soil-induced train loads by using 2.5D FEM and analyzed the effects of track irregularity on ground vibration. Alves Costa et al. [27, 28] established a 2.5D FEM-BEM model of roadbed-soil structure, considering the train-track dynamic interaction, and validated the correctness of the model by the field vibration tests. Villalba Sanchis et al. [29] studied the dynamic responses of a dual gauge track induced by the train passage by experimental and numerical investigations. In order to accurately analyze vibration characteristics and site effects of loess hills under the moving load of a high-speed train, Yan et al. [30] established four types of loess hill models under railway viaduct by the finite element analysis software by field test, the dynamic response and stability of loess hills under two different vibration sources under high-speed train load were studied by using two-dimensional equivalent linear response time history analysis, and the influence of the mechanical parameters of loess on the vibration of different types of loess hill was analyzed.

From the above studies, it can be seen that the research on vibration caused by train operation is mainly focused on flat sites in soft soil, permafrost, and loess areas, and there is less research on the vibration characteristics of complex terrain landforms along railroad lines. The role of topography has been considered by scholars in the field of earthquake engineering [31, 32], and it is found that topography makes the vibration propagation characteristics significantly different from those of a flat site. However, there are significant differences between the characteristics of vibrations caused by high-speed trains and ground vibrations in the time and frequency domains. The Bao-Lan high-speed railway is the main component of the "eight horizontal and eight vertical" high-speed passenger transportation network in China, and one-third of the total length of the railroad is located in the Tianli basin, where the loess layer thickness is large, the wetness level is high, and there are complex topographical features such as tableland, beam, and hill [33].

Due to the very complex geomorphology of the Loess Plateau, there are not only roadbeds but also a large number of bridges and tunnels along the railroad line. Meanwhile, quite a number of previous studies did not consider the effects of different sites and landforms on vibration propagation. In order to accurately analyze the vibration characteristics of loess hilly sites under high-speed train operating loads and their site effects, a series of field vibration tests were conducted in this work based on the site test profiles, and a finite element (FE) model of loess hilly sites under high-speed railroad viaducts was established. The two-dimensional equivalent linear response time dynamic analysis method is used to study and analyze the dynamic response of the loess hilly site under the vibration source of the train operating load and its stability under the high-speed train load. The vibration propagation characteristics, attenuation law, and spectral characteristics of the loess hilly site from the field test and numerical simulation are compared and analyzed, and the vibration characteristics of the bridge piers and surrounding sites along the Baolan high-speed railroad are studied. The study is of great help to the stability and safety prediction of railroad projects in loess areas.

2. Field Testing

2.1. Testing Instruments. The ground vibration test instrument used is an 891-II type vibration meter (Figure 1), which is developed by the Institute of Engineering Mechanics of China Earthquake Bureau and can be used to test ground vibration, pulsation or vibration of building structures, and engineering vibration. The vibrometer is mainly composed of a geophone and a SysCom data acquisition system, which mainly includes amplifiers, recorders, filters, and data acquisition instruments. This instrument has the characteristics of small size, lightweight, easy to carry and use, and large test range. The acceleration test range of this instrument is 0~2.0 g, the sampling interval is 0.005 s, and the recording length of this instrument is 5 s before the excitation and 35 s after the excitation.

In this test, the *X* direction is specified as the direction of train operation, the *Y* direction is perpendicular to the line direction, and the *Z* direction is the direction of gravity.

2.2. Loess Hill Site Environment and Measurement Point Layout. The test site is located under an elevated bridge of Qin'an-Tongwei on the Baolan passenger dedicated line, with a bridge height of about 20 m. One side of the bridge is a flat terrain, while the other side is a typical rectangular loess hill terrain. In the vertical direction of the high-speed railway bridge at a distance of 41 m on the side of the rectangular loess hills were arranged with a total of six measurement points, of which measurement point 1 was arranged at a distance of 2 m from the bridge abutment, measurement point 2 was arranged at a distance of 9 m from the bridge abutment, measurement point 3 was arranged at a distance of 18 m from the bridge abutment, measurement point 4 was arranged at a distance of 27 m from the bridge abutment, and measurement points 5 and 6 were arranged on the loess hill site, which was 30 m and 41 m away from the bridge abutment, respectively. The width of the loess hill site was 11 m. The height was 4.5 m. The measurement point layout and the shape of loess hill are shown in Figure 2.

3. Numerical Simulation

3.1. Numerical Simulation Methods: Finite Element and Infinite Element Coupled Analysis Methods

3.1.1. Finite Element Analysis Methods. The finite element unit method is an essential tool for engineering structural analysis and large-scale numerical calculations, and the emergence of the finite element method is an important breakthrough in the field of numerical calculations. The basic method is to divide the finite area into a finite number of units, establish algebraic control equations on each unit and solve them, and then connect these divided units in a certain way, and the format of the divided units can be various shapes, so it can be used to solve the calculation of complex models.

Dynamic analysis is different from statics, when the building structure receives a load, and the magnitude and direction of the load are related to time, which requires that not

FIGURE 1: 891-II vibration meter.

only the magnitude of the inertia force but also the influence of damping should be considered in the dynamic analysis. At present, two methods can be used for solving dynamics problems, which are explicit and implicit solutions.

In order to understand the dynamic characteristics of a structure, such as a building, during the whole vibration process, it is necessary to use the time course analysis method to solve the problem. The time course analysis method is used to solve the differential equations of motion of the object by numerical methods of stepwise integration and finally to find out the motion of the structure and building during the whole vibration process.

3.1.2. Infinite Element Analysis Method. In geotechnical engineering, the community foundation is actually a semi-infinite space structure, which should be considered as infinite when calculating and analyzing. However, in the dynamic analysis of geotechnical engineering, it is generally only concerned with the vibration in and around the building structures and does not need to be considered infinitely far away, so it is reduced to a near-field fluctuation problem.

In the numerical calculation model, it is impossible to build the foundation as an infinite area, and it is necessary to truncate it, but on the truncated boundary, the vibration wave will have an obvious bouncing effect, which is obviously not consistent with the actual situation, resulting in errors in the results of numerical calculation. In order to solve this problem, ABAQUS provides a new method, namely, infinite elements to meet the needs of the calculation. The definition of an infinite element in ABAQUS can only be rewritten by inp file, and the unit name of the infinite element contains "IN."

3.2. Site Model and Soil Parameters of Loess Hill Site under Viaduct of High-Speed Railroad. In order to study the influence of rectangular loess hill site and soil mechanical parameters on vibration propagation under the elevated bridge, and the vibration characteristics of different forms of loess hill site, a rectangular loess hill model consistent with the site was established according to the field measurement profile: the length of the rectangular loess hill is 11 m.

The length of the rectangular loess hill is 11 m, and the width is 4.5 m, as shown in Figure 3. The model is divided into two parts, the first part is the bridge pier and pile

(a)
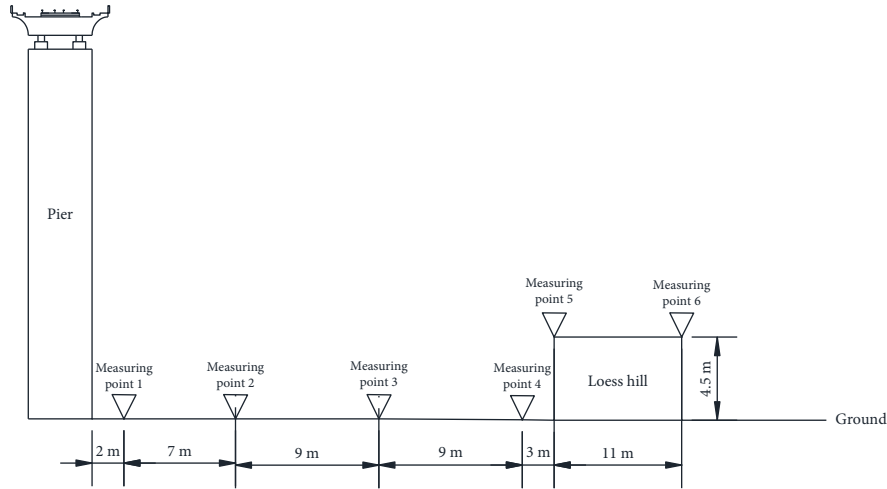
(b)

FIGURE 2: Schematic diagram of site and measuring points of rectangular loess hill site under the railway viaduct. (a) Field layout of vibration measuring points at the loess hill site under the railway viaduct. (b) Layout diagram of vibration measuring points at the loess hill site under the railway viaduct.

foundation, the pier height is 20 m, the width is 4 m, using bored piles and two pile foundations, and pile length is 8 m, using C30 concrete; the second part is the loess body because the acceleration and displacement of the foundation vibration caused by the train are usually small, the soil body is considered elastic, its physical and mechanical parameters are shown in Table 1 [34], and the thickness of the loess is 40 m. The left and right boundaries of loess body model are used as infinite element boundaries in order to prevent the reflection effect of waves.

In order to compare with the field test data, a total of six measurement points are arranged on the side of the rectangular loess hill under the bridge of the model structure, all of which are consistent with the location of the field test points: measurement point 1 is arranged 2 m from the bottom of the bridge pier, measurement point 2 is 9 m from the bottom of the bridge pier, measurement point 3 is 18 m from the bottom of the bridge pier, measurement point 4 is 27 m from the bottom of the bridge pier, measurement point 5 is arranged on the left side of the rectangular loess hill, and the horizontal distance of measurement point 4 is 3 m. The width of the loess hill is 11 m, the height is 4.5 m, and the measurement point 6 is arranged on the right side of the rectangular loess hill, which is 41 m from the bottom of the bridge pier, as shown in Figure 3. The finite element grid cell size is 1 m × 0.5 m, total of 7639 grids.
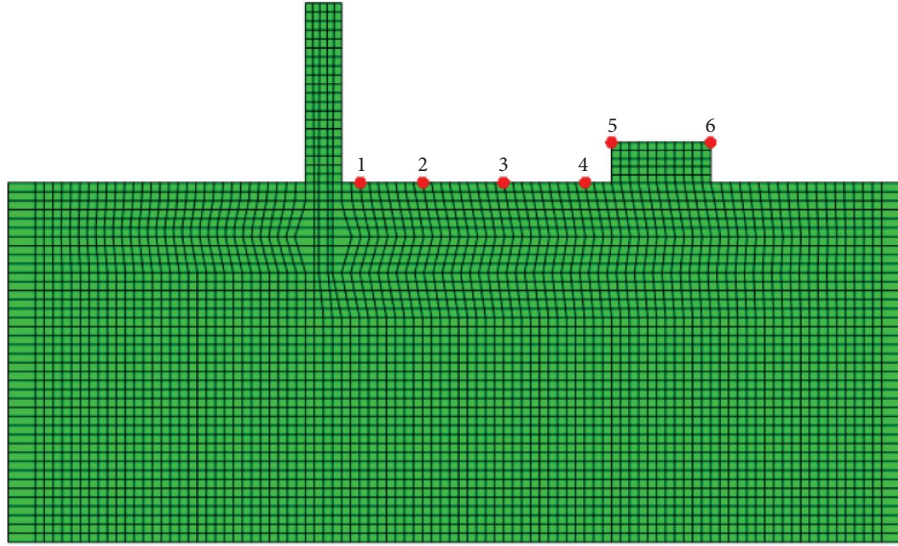
Figure 3: Model of loess hill site.

Table 1: Parameters of the soil layer in the loess site.

Soil layer no.	Soil layer type	Thickness (m)	Depth (m)	Density (kg/m^3)	Modulus of elasticity (MPa)	Poisson's ratio
1	Loess	5.0	5.0	1550	50.22	0.30
2	Loess	5.0	10.0	1600	64.00	0.30
3	Loess	5.0	15.0	1630	86.23	0.30
4	Loess	5.0	20.0	1650	129.36	0.30
5	Loess	5.0	25.0	1680	151.20	0.30
6	Loess	5.0	30.0	1700	182.95	0.30
7	Loess	10.0	40.0	1700	208.25	0.30

3.3. Model Vibration Load. Figure 4(a) shows the vibration waveform of the vertical direction (*z*-component) at the location of the abutment bearing platform recorded by the vibration test during the passage of a 16-section train with a speed of 240 km/h of the Baolan high-speed railroad, which is the vibration load applied by the numerical calculation. Before application, high-pass filtering and baseline correction were performed by Seismosignal software to filter out the components of seismic waves with frequencies less than 0.1 Hz. The vibration duration used for the calculation is 10.00 s, and the maximum peak acceleration is 51.27 cm^2/s. Figure 4(b) shows the vibration Fourier spectrum characteristics, and the vibration duration applied for the calculation is dominated by the medium and high-frequency components, and the excellence frequency is 15 Hz. Figure 4(c) shows the vibration energy spectrum curve with a remarkable frequency of 15 Hz.

3.4. Stability Analysis of the Rectangular Loess Hill Site under the Viaduct. Since the loess hill site and its surrounding sites are mainly subject to the action of gravity under natural conditions, their stability is mainly controlled by gravity, while the construction of the railroad viaduct in its vicinity is subject to the coupled action of gravity and train load due to

the influence of train operation. Therefore, in order to further analyze the characteristics of the loess hill site elevated under the coupling action of train load and gravity, the maximum vertical displacement clouds under the action of train load and gravity, and the Mises stress clouds under the coupling action of train load and gravity were compared and analyzed, as shown in Figures 5 and 6.

As can be seen from Figure 5, the vertical maximum displacement clouds under gravity load are significantly different from those under train load. Under gravity, the vertical displacement under the viaduct is larger, and the maximum vertical displacement decreases with the increase of depth and distance from the bottom of the bridge pier; while the vertical displacement of the loess hill is the largest, and again, the maximum vertical displacement is decaying with the increase of depth and distance from the loess hill. Also, under the action of train load, the vertical displacement only occurs around the bridge pier and has no effect on the vertical displacement of the loess hill basically.

As can be seen from Figure 6, there is basically no difference between the Mises stress clouds under gravity and under the coupling of train load and gravity, except that under the coupling of train load and gravity, there is a significant increase in the Mises stress applied to the pile foundation and its bottom soil.
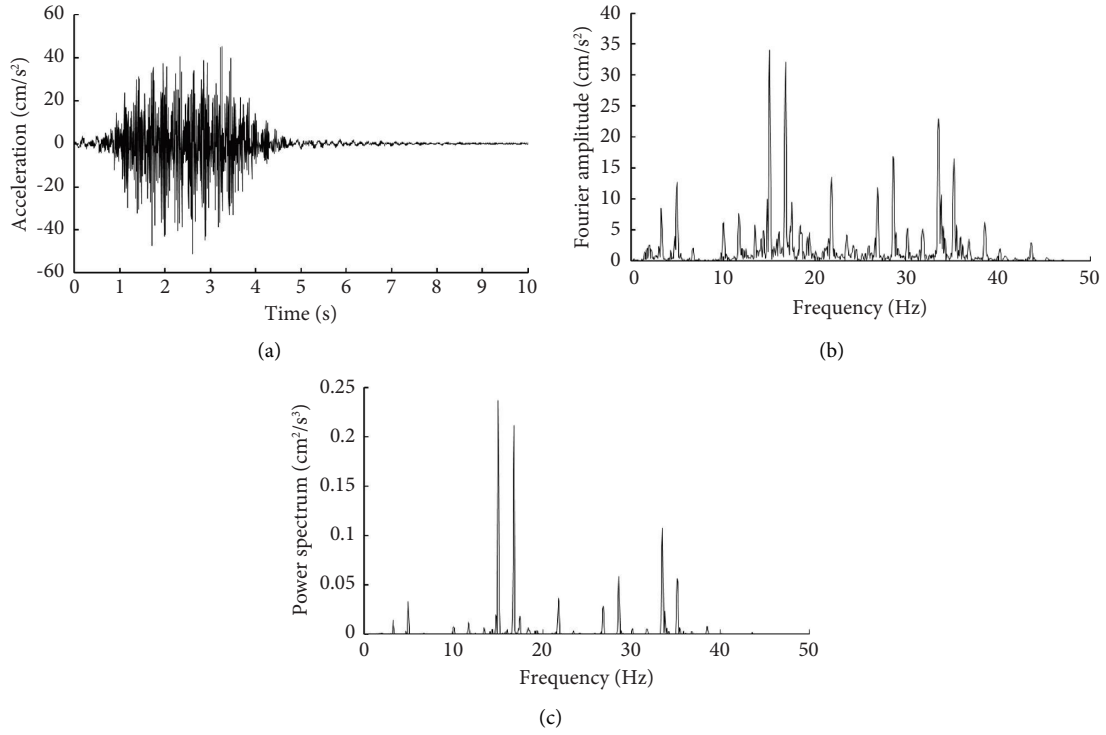
(a)

(b)

(c)

FIGURE 4: Numerical calculation of the input vibration acceleration time range and its spectrum curve.
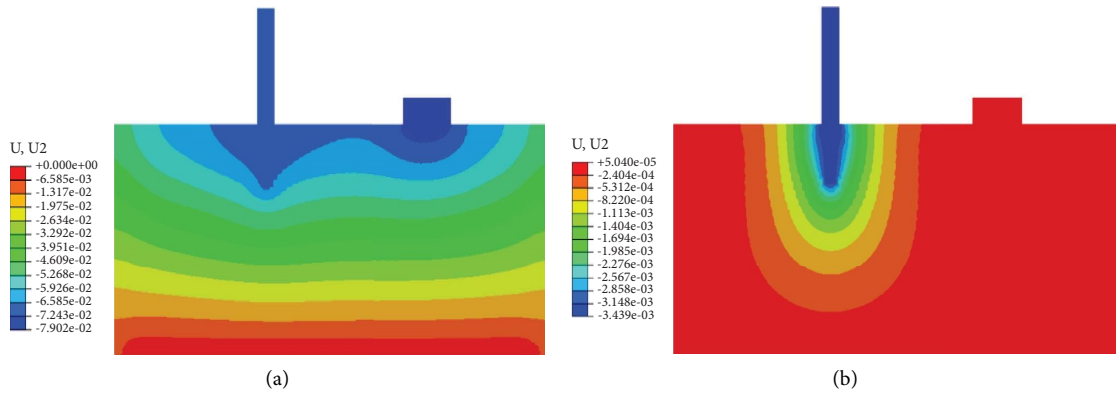

(a)

(b)

FIGURE 5: Comparison of maximum displacement clouds. (a) The vertical maximum displacement cloud of the loess hill site under the viaduct under gravity load. (b) The vertical maximum displacement cloud of the loess hill site under the viaduct under the high-speed train load.
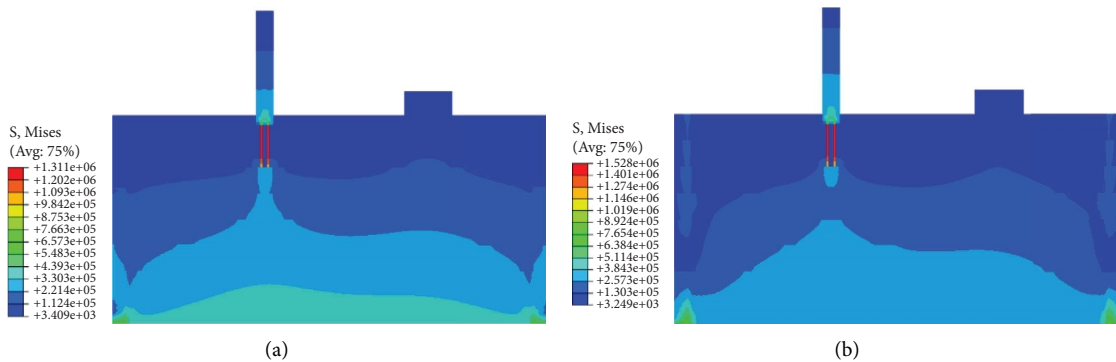

(a)

(b)

FIGURE 6: Mises comparison of stress clouds. (a) Mises stress clouds of the rectangular loess hill site under the viaduct under gravity load. (b) Mises stress clouds of the rectangular loess hill site under the viaduct with coupled gravity and train loads.

3.5. Numerical Simulation Acceleration Clouds. Figures 7 and 8 show the vibration acceleration clouds of the loess site under the same viaduct at different moments, respectively. From the figures, it can be seen that the vibration acceleration distribution clouds of the loess hill site at different moments (6.68 s and 6.89 s) are similar, and the vibration acceleration all gradually decreases with the increase of the vibration source distance, but the acceleration all shows a significant increase on the loess hill site.

4. Comparison Analysis of Field Test and Numerical Simulation Results

4.1. Acceleration Time Range. Figure 9 shows the vertical (z-component) vibration acceleration time course of each observation point 1 to 6 in the loess site under the viaduct during the passage of a 16-section train with a speed of 242 km/h of the high-speed railroad, and it can be seen that the ground vibration acceleration waveform of each observation point in the loess site has similarity, and there is good symmetry above and below the vibration acceleration time course curve of each measurement point, and there are obvious periodic peaks, and the vibration in the loess hill. The amplification effect is very obvious.

As can be seen from the figure, the peak vibration accelerations of measurement points 1 to 6 recorded in the field test are 18.74 cm/s^2, 12.24 cm/s^2, 9.67 cm/s^2, 8.56 cm/s^2, 11.26 cm/s^2, and 12.81 cm/s^2, respectively, and the peak vibration accelerations of measurement points 1 to 6 recorded in the numerical simulation are 19.49 cm/s^2, 15.46 cm/s^2, 15.73 cm/s^2, 10.94 cm/s^2, 13.03 cm/s^2, and 14.89 cm/s^2, respectively, and it is obvious that the peak vibration acceleration of measurement points 1~4 decays with distance as they are farther away from the bridge pier, while on the rectangular loess hill due to the influence of site conditions, which makes the peak vibration acceleration of measurement point 5 and measurement point 6 appear "rebound increase", the data recorded in the field test are 1.32 times and 1.49 times magnified, respectively, compared to measurement point 4, and the data recorded in the numerical simulation are 1.19 times and 1.36 times magnified, respectively, compared to measurement point 4. At the same time, the vibration durations of measurement points 1 to 4 recorded in the field test were all 7.5 s, while the vibration durations of measurement points 5 and 6 were both 8.81 s. Both showed an increase in vibration duration, which were amplified by 1.17 times compared with the first four measurement points.

Figure 10 shows the peak vertical (z-component) vibration acceleration curves, amplification coefficients, and $a_{\text{Simulated-max}}/a_{\text{Observed-max}}$ values for each observation point 1 to 6 at the loess site under the viaduct during high-speed railroad train operation recorded by field tests and numerical simulations. From the figure, it can be seen that the peak vibration acceleration of measurement points 1 to 4 recorded by both field test and numerical simulation decayed linearly with distance, while measurement point 5 and measurement point 6 showed amplification

phenomenon, and the overall peak value of numerical simulation was larger than that of field test (Figure 10(a)). Figure 10(b) shows the amplification factor obtained from the ratio of the peak acceleration at each measurement point to the peak acceleration at measurement point 1 in the field test. Figure 10(b) shows the amplification coefficient of the peak acceleration of each measurement point and the amplification coefficient of the peak acceleration of measurement point 1, $a_{\text{Simulated-max}}/a_{\text{Observed-max}}$ values range from 1.04 to 1.63, with the largest dispersion at measurement point 3, and $a_{\text{Simulated-max}}/a_{\text{Observed-max}}$ values at the other five measurement points range from 1.04 to 1.28. This indicates that there is still some error between the numerically simulated soil parameters and the real soil parameters.

4.2. Spectrum Analysis

4.2.1. Spectrum Analysis Method of Strong Vibration. Spectral analysis of data from strong vibration observations is actually a process of Fourier transform and Fourier inverse transform. The value of N (even) of the time function at equal time interval points x_m ($m = 0,1,2,...,N-1$):

$$A_k = \frac{2}{N}\sum_{m=0}^{N-1} x_m \cos\frac{2\pi km}{N} \quad k = 0,1,2,\ldots,\frac{N}{2}-1,\frac{N}{2}$$

$$B_k = \frac{2}{N}\sum_{m=0}^{N-1} x_m \sin\frac{2\pi km}{N} \quad k = 1,2,\ldots,\frac{N}{2}-1, \tag{1}$$

where x_m is denoted as a finite trigonometric function with A_k and B_k as coefficients.

$$x_m = \frac{A_0}{2} + \sum_{k=1}^{N/2-1}\left[A_k \cos\frac{2\pi km}{N} + B_k \sin\frac{2\pi km}{N}\right]$$

$$+ \frac{A_{N/2}}{2}\cos\frac{2\pi(N/2)m}{N}. \tag{2}$$

Considering that this function is nothing but an approximation of the metric function x_t.

$$\tilde{x}(t) = \frac{A_0}{2} + \sum_{k=1}^{N/2-1}\left[A_k \cos\frac{2\pi kt}{N\Delta t} + B_k \sin\frac{2\pi kt}{N\Delta t}\right]$$

$$+ \frac{A_{N/2}}{2}\cos\frac{2\pi(N/2)t}{N\Delta t}. \tag{3}$$

Equation (3) is a finite Fourier approximation of the function x_t. The coefficients A_k and B_k in equation (1) are of finite Fourier coefficients. The calculation of equation (1) is called the Fourier transform of the discrete value x_m, and the calculation of equation (2) is called the Fourier inverse transform.

Here, the introduction of the complex Fourier coefficients C_k is

$$x_m = \sum_{k=0}^{N-1} C_k e^{i(2\pi km)} \quad m = 0,1,2,\ldots,N-1. \tag{4}$$
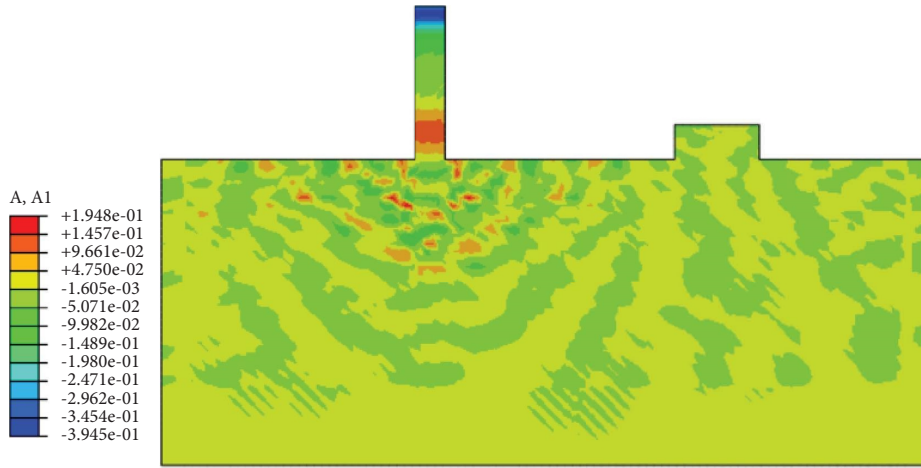
Figure 7: Acceleration clouds of the loess site under the viaduct at $t = 6.68$ s.
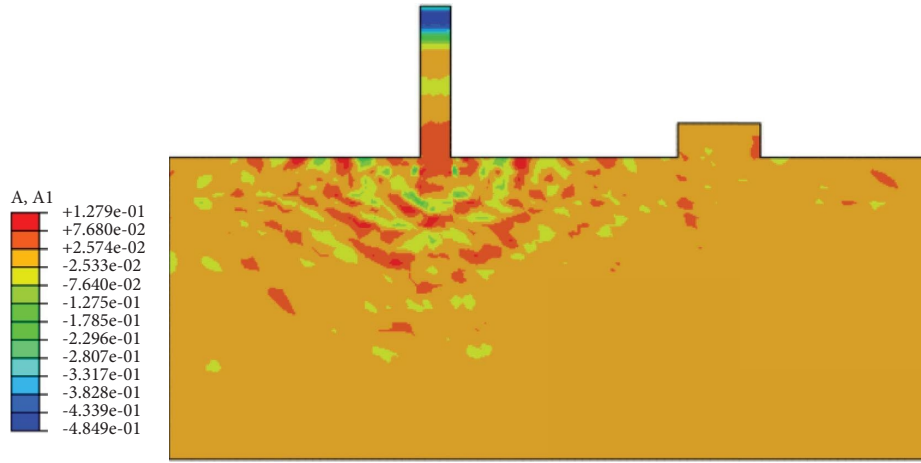

Figure 8: Acceleration clouds of the loess site under the viaduct at $t = 6.89$ s.

In a more concise way, it can be expressed as the following equation, called the finite complex Fourier series,

$$C_k = \frac{1}{N} \sum_{m=0}^{N-1} x_m e^{-i(2\pi km/N)} \quad k = 0,1,2,\ldots,N-1. \quad (5)$$

Equation (4) is the Fourier transform, and equation (5) is the inverse Fourier transform. Using the above calculation method, the observed data can be subjected to spectral analysis.

4.2.2. Fourier Spectrum. From Figure 11, it can be seen that the Fourier spectrum waveforms of each measurement point recorded by numerical simulation and field test have similarity and have obvious periodic peaks, the amplification of vibration in the loess hill is very obvious, and the overall amplitude and peak acceleration are similar to the linear decay with distance, and the amplification phenomenon is presented at measurement point 5 and measurement point 6. The Fourier spectrum frequencies recorded by numerical simulation and field test are mainly concentrated in 1~40 Hz when the train with the speed of 240 km/h passes by, but the

difference between the main frequencies recorded by the two is large, and the main frequency of Fourier spectrum vibration recorded by numerical simulation is around 15 Hz, which is the same as the main frequency of Fourier spectrum vibration of the input vibration wave, while the main frequency of Fourier spectrum vibration recorded by field test is around 25 Hz. The Fourier spectrum amplitude recorded by numerical simulation of the same measurement point is larger than the amplitude recorded by the field test, and the Fourier spectrum frequency range of measurement points 3~6 recorded by the field test is larger between 1 and 45 Hz, while the Fourier spectrum frequency range of measurement points 3~6 recorded by numerical simulation is between 1 and 25 Hz.

From Figure 12, it can be seen that the Fourier spectrum amplitudes of measurement points 1 to 6 recorded in the field test are 11.95 cm/s^2, 7.68 cm/s^2, 6.23 cm/s^2, 6.75 cm/s^2, 8.45 cm/s^2, and 9.62 cm/s^2, respectively, and the Fourier spectrum amplitudes of measurement points 1 to 6 recorded in the numerical simulation are 13.82 cm/s^2, 20.53 cm/s^2, 22.64 cm/s^2, 13.95 cm/s^2, 16.53 cm/s^2, and 16.83 cm/s^2, respectively, and it is obvious that the Fourier spectrum
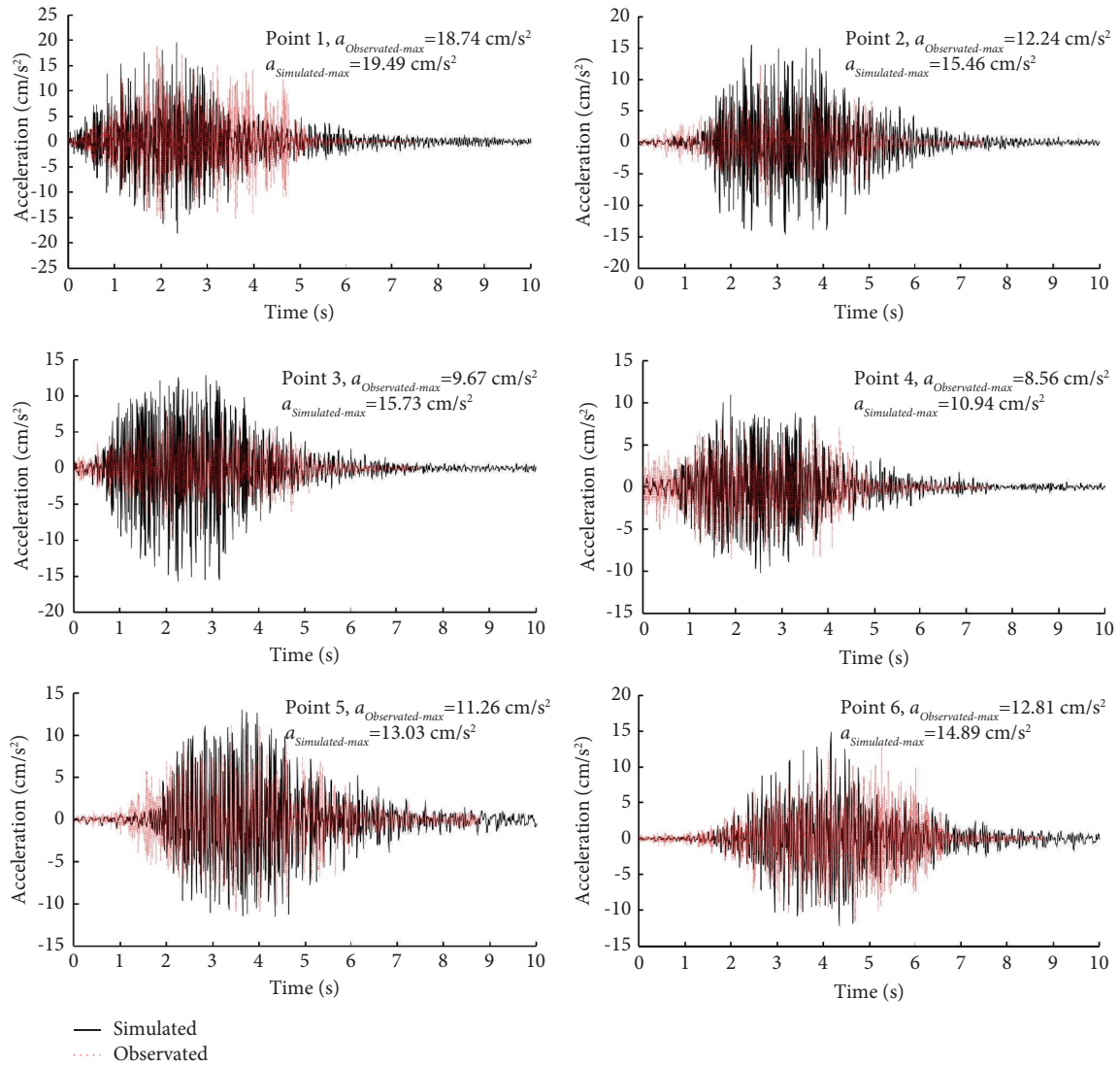
Figure 9: Time course of vertical vibration acceleration for each observation point in field test and numerical simulation.
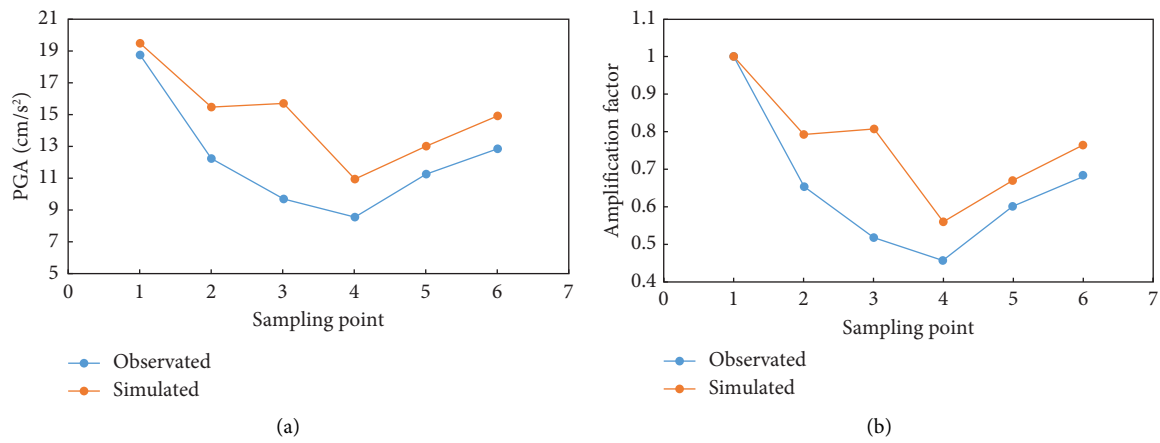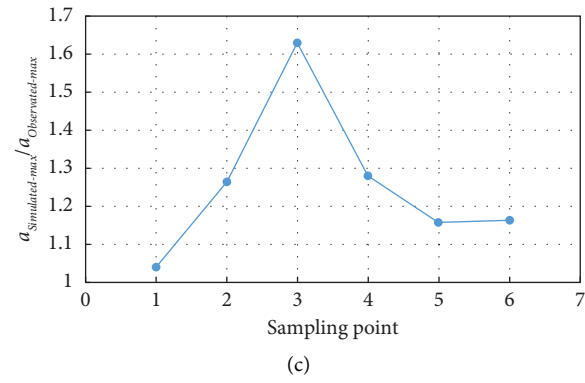

(a)

(b)

Figure 10: Continued.

(c)

Figure 10: Comparison of acceleration peak at each measurement point between field test and numerical simulation.
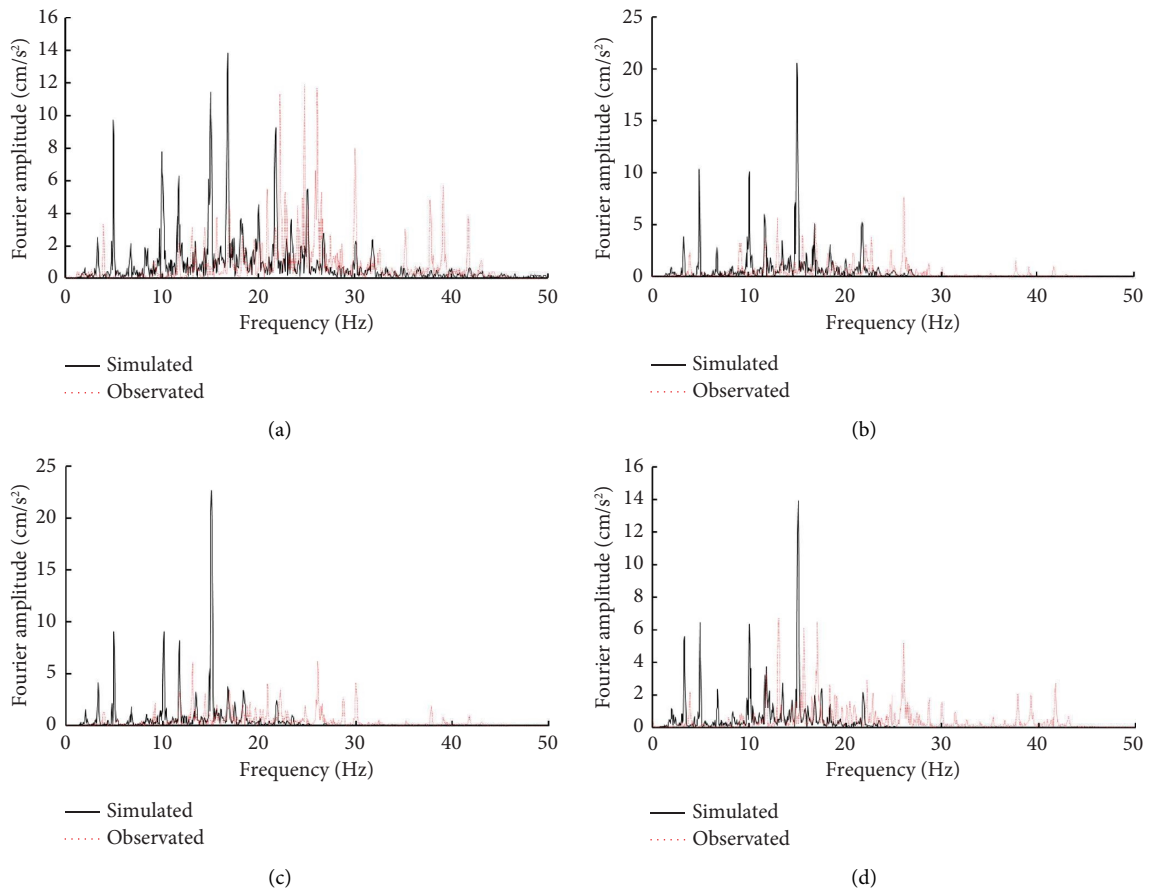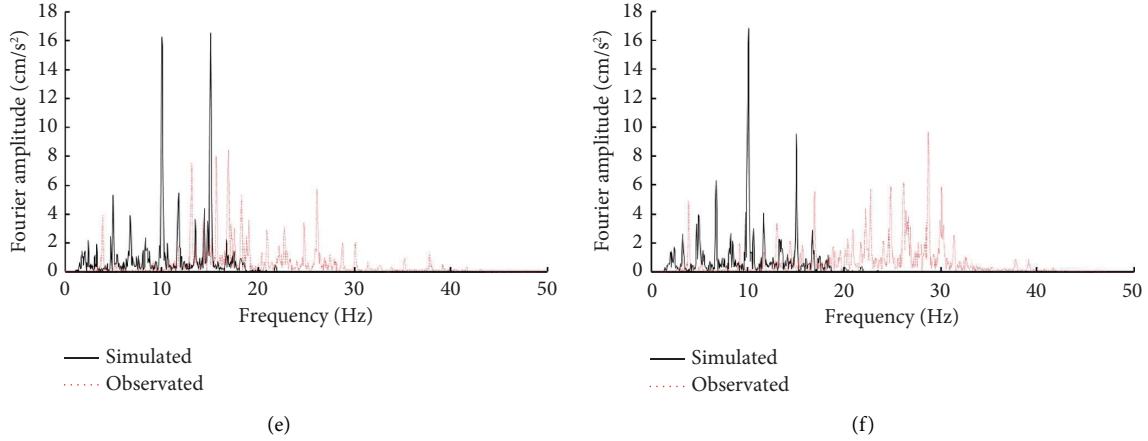

(a)

(b)

(c)

(d)

Figure 11: Continued.

(e)

(f)

FIGURE 11: Fourier spectrum of each measurement point for field test and numerical simulation. (a) Point 1. (b) Point 2. (c) Point 3. (d) Point 4. (e) Point 5. (f) Point 6.
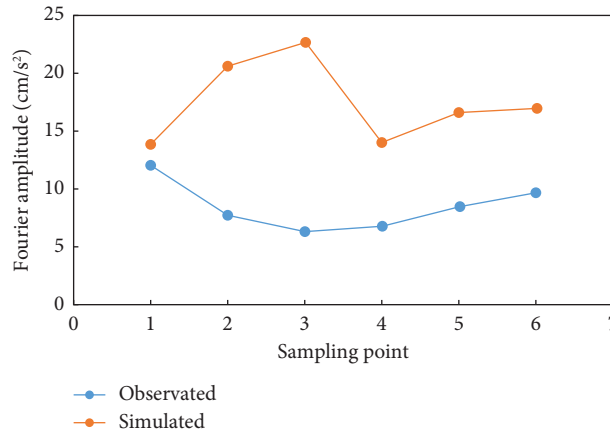

FIGURE 12: Comparison of Fourier spectrum amplitude at each measurement point between field test and numerical simulation.

amplitudes of measurement points 1~4 decay with distance as they are farther away from the piers, while on the rectangular loess hill due to the influence of site conditions, making the Fourier spectrum amplitudes of measurement point 5 and measurement point 6 appear "rebound increase," the data recorded in the field test are amplified 1.25 times and 1.43 times compared to measurement point 4, and the data recorded in the numerical simulation are amplified 1.19 times and 1.21 times compared to measurement point 4.

4.2.3. Energy Spectrum. The vibration acceleration energy spectrum reflects the distribution of vibration acceleration energy at individual frequencies, and the relationship between the acceleration energy spectrum function $G(\omega)$ and the spectrum function $f(j\omega)$ can be expressed as follows [35]:

$$G(\omega) = |f(j\omega)|^2. \qquad (6)$$

In order to further analyze the relationship between the vibration characteristics of each measurement point and the distance from the vibration source, the vibration acceleration signals of each measurement point recorded by numerical simulation and field test were analyzed by energy spectrum, as shown in Figures 13 and 14.

From Figure 13, it can be seen that the energy spectrum waveforms of each measurement point recorded by numerical simulation and field test have similarities and have obvious periodic peaks. When a train with an hourly speed of 240 km/h passes by, the frequencies of the energy spectrum recorded by the numerical simulation and the field test are mainly concentrated in the range of 1~40 Hz, but the difference between the main frequencies recorded by the two is large. The amplitude of the energy spectrum recorded by the numerical simulation is larger than that recorded by the field test, and the frequency range of the energy spectrum of measurement points 3~6 recorded by the field test is larger between 1 and 30 Hz, while the frequency range of the Fourier spectrum of measurement points 3~6 recorded by the numerical simulation is between 1 and 20 Hz.

As can be seen from Figure 14, the energy spectrum amplitudes of measurement points 1 to 6 recorded in the field test are 0.17 cm^2/s^3, 0.26 cm^2/s^3, 0.18 cm^2/s^3, 0.19 cm^2/s^3, 0.19 cm^2/s^3, and 0.21 cm^2/s^3, respectively, and the energy
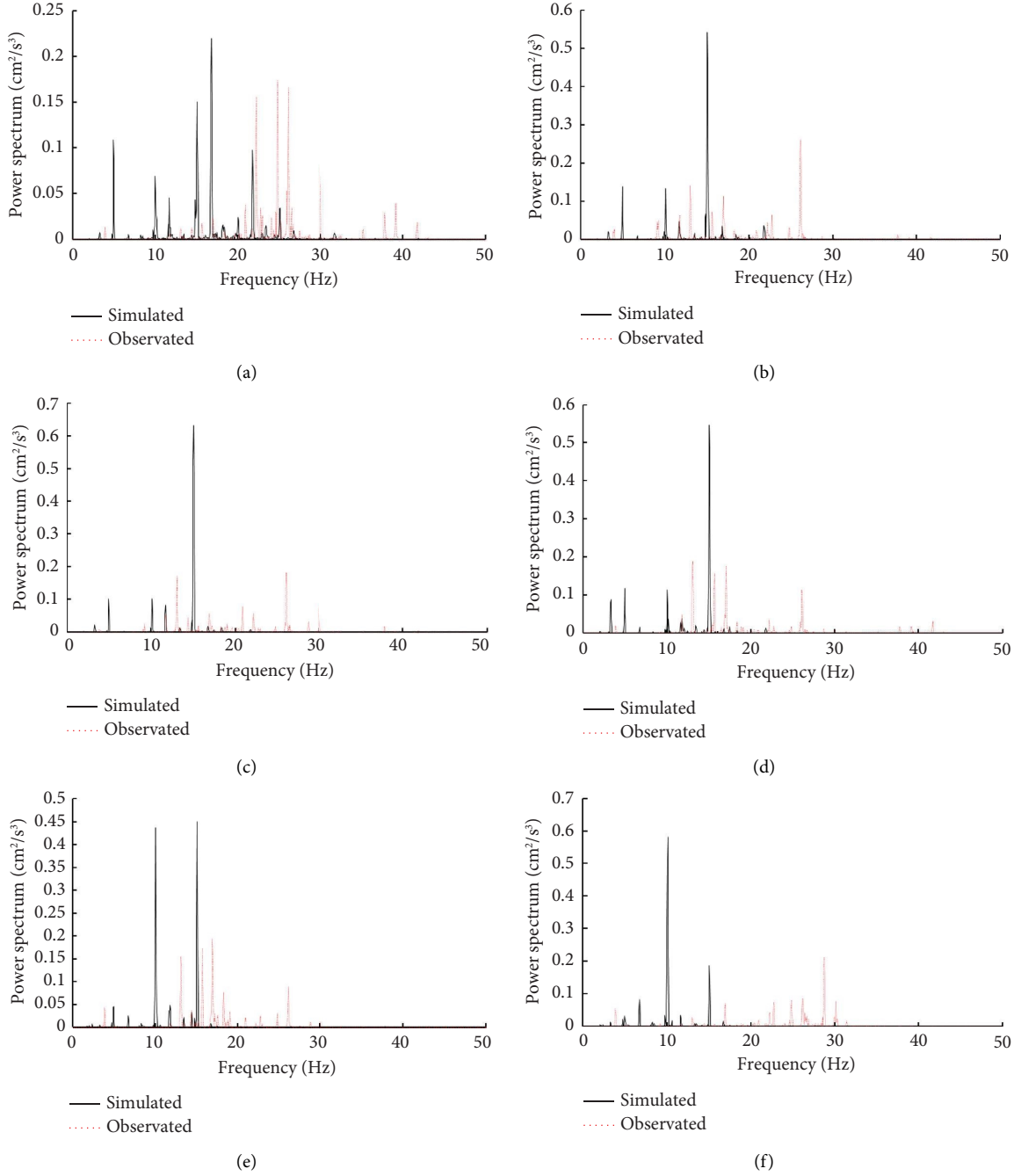
FIGURE 13: Energy spectrum of each measurement point from field test and numerical simulation. (a) Point 1. (b) Point 2. (c) Point 3. (d) Point 4. (e) Point 5. (f) Point 6.

spectrum amplitudes of measurement points 1 to 6 recorded in the numerical simulation is $0.22 \, cm^2/s^3$, $0.54 \, cm^2/s^3$, $0.63 \, cm^2/s^3$, $0.55 \, cm^2/s^3$, $0.45 \, cm^2/s^3$, and $0.58 \, cm^2/s^3$, and the energy spectra of measurement point 1 are the smallest,

the data recorded in the field test are 1.11 times larger than that of measurement point 4, and the data recorded in the numerical simulation are 1.05 times larger than that of measurement point 4.
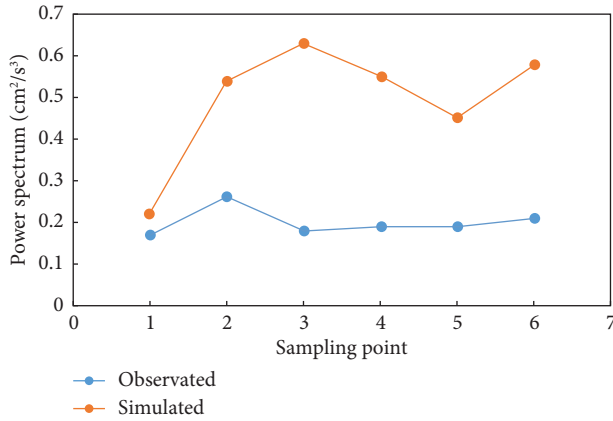
Figure 14: Comparison of energy spectrum amplitude at each measurement point between field test and numerical simulation.

5. Conclusion

Through the field vibration test and numerical simulation of the loess hill site during the passage of the train of the Baolan high-speed railway, the following conclusions were obtained based on the comparative analysis and research in both time and frequency domains:

(1) The vertical maximum displacement clouds under the action of gravity load and train load are obviously different. Under the action of gravity, the vertical displacement under the elevated bridge is larger, and the maximum vertical displacement decreases with the increase of depth and distance from the bottom of the bridge pier while the vertical displacement of the loess hill is the largest, and again, the maximum vertical displacement is decaying with the increase of depth and distance from the loess hill. Also, under the action of train load, the vertical displacement only occurs around the bridge pier and has no effect on the vertical displacement of the loess hill basically. There is basically no difference between the Mises stress clouds under gravity and the coupled train load and gravity, except that the Mises stress on the pile foundation and its bottom soil increases significantly under the coupled train load and gravity.

(2) The vibration acceleration distribution clouds of the loess hill site at different moments are similar, and the vibration acceleration all gradually decreases with the increasing distance of the vibration source, but the acceleration on the loess hill all shows a significant increase. The waveform of ground vibration acceleration at each observation point of the loess site has similarity, and there is good symmetry above and below the time course curve of vibration acceleration at each measurement point, there is an obvious periodic peak, and the vibration amplification in the loess hill is very obvious, and the ratio of peak acceleration at each measurement point is recorded by numerical simulation and field test, the

$a_{\text{Simulated-max}}/a_{\text{Observed-max}}$ values range from 1.04 to 1.63, with the largest dispersion at measurement point 3, and the $a_{\text{Simulated-max}}/a_{\text{Observed-max}}$ values at the other five measurement points range from 1.04 to 1.28, generally showing that the peak acceleration recorded by the numerical simulation is larger than that of the field test. The vibration durations of measurement points 1 to 4 recorded in the field test were all 7.5 s, while the vibration durations of measurement point 5 and measurement point 6 at the location of the loess hill site were both 8.81 s. Both showed an increase in vibration duration, which was 1.17 times larger than the previous four measurement points, respectively.

(3) When a high-speed train with a speed of 240 km/h passes through, the Fourier spectrum frequencies recorded by numerical simulation and field test are concentrated between 1 and 40 Hz, but the difference of the main frequency between the two records is large, the main frequency of Fourier spectrum vibration recorded by numerical simulation is 15 Hz, which is the same as that of the input vibration waveform, but the main frequency of Fourier spectrum vibration recorded by field test is 25 Hz; as the distance from the bridge abutment gets farther and farther away, the Fourier spectrum amplitude of the loess flat site in the non-loess hills gradually decays with the distance, whereas the Fourier spectrum amplitude is amplified in the loess hill site due to the site condition.

(4) When the train with the speed of 240 km/h passes by, the energy spectrum frequencies recorded by numerical simulation and field test are mainly concentrated in 1~40 Hz, but the difference between the main frequencies recorded by the two is large, the main frequency of energy spectrum vibration recorded by numerical simulation is around 15 Hz, which is the same as the main frequency of energy spectrum vibration of the input vibration wave, while the main frequency of energy spectrum vibration recorded by field test is around 25 Hz. The energy spectrum of measurement point 1 is the smallest, and the energy spectrum of measurement points 2~5 decays with distance as the distance from the bridge pier gets farther, but the energy spectrum of measurement point 6 has a "rebound increase," and the data recorded in the field test are 1.11 times larger than that of measurement point 4, and the data recorded in the numerical simulation are 1.05 times larger than that of measurement point 4.

(5) Through the comparative analysis of the results of the field vibration test and numerical calculation of the Baolan high-speed railway, it is found that the results obtained from the field vibration test and numerical calculation of the high-speed railway have high similarity, which can provide the corresponding basis for the theoretical analysis of the vibration effect of the loess site of train vibration, verify the

correctness and applicability of the theoretical model and numerical analysis model, and can evaluate the environmental vibration caused by the train and predict the train vibration. It can also provide a basis for the assessment of train-induced environmental vibration and the prediction of train vibration.

Data Availability

The data used to support the findings of the article are included within the article.

Conflicts of Interest

The authors declare that they have no conflicts of interest.

Acknowledgments

References

[1] V. V. Krylov, "On the theory of railway-induced ground vibrations," *Journal de Physique IV*, vol. 4, no. 5, 1994.

[2] V. V. Krylov, A. R. Dawson, M. E. Heelis, and A. C. Collop, "Rail movement and ground waves caused by highspeed trains approaching track-soil critical velocities," *Proceedings of the Institution of Mechanical Engineers, Part F: Journal of Rail and Rapid Transit*, vol. 214, no. 2, pp. 107–116, 2000.

[3] X. Sheng, C. J. C. Jones, and D. J. Thompson, "A comparison of a theoretical model for quasi-statically and dynamically induced environmental vibration from trains with measurements," *Journal of Sound and Vibration*, vol. 267, no. 3, pp. 621–635, 2003.

[4] W. Zhai, K. Wang, and C. Cai, "Fundamentals of vehicle-track coupled dynamics," *Vehicle System Dynamics*, vol. 47, no. 11, pp. 1349–1376, 2009.

[5] Y. Cai, H. Sun, and C. Xu, "Steady state responses of poroelastic half-space soil medium to a moving rectangular load," *International Journal of Solids and Structures*, vol. 44, no. 22-23, pp. 7183–7196, 2007.

[6] X. Lei and B. Zhang, "Analysis of dynamic behavior for slab track of high-speed railway based on vehicle and track elements," *Journal of Transportation Engineering*, vol. 137, no. 4, pp. 227–240, 2011.

[7] H. Xia, N. Zhang, and C. A. O. Yan-mei, "Experimental study of train-induced vibrations of ground and nearby buildings," *Journal of the China Railway Society*, vol. 26, no. 4, pp. 93–98, 2004.

[8] G. Gao, L. I. Zhi-yi, and F. E. N. G. Shi-jin, "Experimental results and numerical predictions of ground vibration induced by high-speed train running on Qin-Shen railway," *Rock and Soil Mechanics*, vol. 28, no. 9, pp. 1817–1822, 2007.

[9] J. Chen, H. Xia, and J. Xiao, "Experimental study of ground vibrations induced by moving train," *Rock and Soil Mechanics*, vol. 29, no. 11, pp. 3113–3118, 2008.

[10] C. H. E. N. Guo-yuan, W. E. I. Li-min, and Y. A. N. G. Guo-lin, "Experimental study on dynamic characteristics of transition section of Hujiatun Zhongqiao road and bridge," *Journal of Vibration and Shock*, vol. 29, no. 6, pp. 184–188, 2010.

[11] C. H. E. N. Guo-yuan, Y. A. N. G. Guo-lin, and W. E. I. Li-min, "Experimental study on dynamic characteristics of transition section of railway passenger dedicated line culvert," *Journal of Railway Science and Engineering*, vol. 7, no. 1, pp. 47–51, 2010.

[12] L. Zhang, "Test and analysis of vibration induced by elevated railway and snti-vibration measure," *Journal of Railway Engineering Society*, vol. 29, no. 6, pp. 118–125, 2012.

[13] M. Q Xiao, J. Yao, and D. Huang, "Study and field measurement of environmental vibration induced by underground Guangzhou-Shenzhen-Hong Kong high speed rail in Shiziyang tunneL," *Chinese Journal of Rock Mechanics and Engineering*, vol. 23, pp. 3527–3534, 2013.

[14] G. Zhang, *Study on the Ground Vibration Induced by Trains Moving on Subgrade of High-Speed Railway*, Southwest Jiaotong University, Chengdu, China, 2014.

[15] C. H. E. N. Gong-qi, "Ground vibration analysis induced by high-speed train based on in-situ data," *Chinese Journal of Rock Mechanics and Engineering*, vol. 34, no. 3, pp. 601–611, 2015.

[16] M. E. N. G. Xiang-lian and F. J. Zhou, "Spatial analysis and study of roadbed vibration effect on loess area for Xi'an baoji high speed railway," *Journal of Railway Engineering Society*, vol. 34, no. 8, pp. 28–33, 2017.

[17] Z. Wu, T. Chen, and W. Ma, "The creep analysis of plain fill embankment at the permafrost regions along Qinghai-Tibet Railway under train dynamic load," *Rock and Soil Mechanics*, vol. 32, pp. 83–87, 2011.

[18] Z. Wu, T. Chen, and W. Ma, "Characteristics of load transmission of trains in permafrost regions along Qinghai-Tibet railroad," *Chinese Journal of Geotechnical Engineering*, vol. 35, no. Suppl.1, pp. 9–13, 2013.

[19] Z. Wang, L. I. N. G. Xian-chang, and H. U. I. Shu-qing, "Field monitoring of vibration response of subgrade in a seasonally frozen region," *Chinese Journal of Geotechnical Engineering*, vol. 37, no. 9, pp. 1591–1598, 2015.

[20] J. Chen and Y. Zhou, "Dynamic vertical displacement for ballastless track-subgrade system under high-speed train moving loads," *Soil Dynamics and Earthquake Engineering*, vol. 129, 2023.

[21] D. Connolly, A. Giannopoulos, and M. C. Forde, "Numerical modelling of ground borne vibrations from high speed rail lines on embankments," *Soil Dynamics and Earthquake Engineering*, vol. 46, pp. 13–19, 2013.

[22] D. P. Connolly, G. Kouroussis, O. Laghrouche, C. L. Ho, and M. C. Forde, "Benchmarking railway vibrations– track, vehicle, ground and building effects," *Construction and Building Materials*, vol. 92, pp. 64–81, 2015.

[23] G. Degrande, D. Clouteau, R. Othman et al., "A numerical model for ground-borne vibrations from underground railway traffic based on a periodic finite element-boundary

element formulation," *Journal of Sound and Vibration*, vol. 293, no. 3-5, pp. 645–666, 2006.

[24] L. Andersen and C. J. C. Jones, "Coupled boundary and finite element analysis of vibration from railway tunnels- a comparison of two- and three-dimensional models," *Journal of Sound and Vibration*, vol. 293, no. 3-5, pp. 611–625, 2006.

[25] A. Lyratzakis, Y. Tsompanakis, and P. N. Psarropoulos, "Efficient mitigation of highspeed train vibrations on adjacent reinforced concrete buildings," *Construction and Building Materials*, vol. 314, Article ID 125653, 2022.

[26] X. Bian, H. Jiang, C. Chang, J. Hu, and Y. Chen, "Track and ground vibrations generated by high-speed train running on ballastless railway with excitation of vertical track irregularities," *Soil Dynamics and Earthquake Engineering*, vol. 76, pp. 29–43, 2015.

[27] P. Alves Costa, R. Calçada, and A. Silva Cardoso, "Track-ground vibrations induced by railway traffic: in-situ measurements and validation of a 2.5D FEM-BEM model," *Soil Dynamics and Earthquake Engineering*, vol. 32, no. 1, pp. 111–128, 2012.

[28] P. A. Costa and R. Calcada, "Influence of ballast mats on the reduction of track-ground vibrations induced by railway traffic," *Types of Environmental Vibration Tests*, vol. 25, pp. 793–800, 2011.

[29] I. Villalba Sanchis, R. Insa Franco, P. Martínez Fernández, and P. Salvador Zuriaga, "Experimental and numerical investigations of dual gauge railway track behaviour," *Construction and Building Materials*, vol. 299, Article ID 123943, 2021.

[30] W. Yan, H. Zhang, H. Z. Zheng, Z. Wu, and X. X. Tian, "Numerical modelling of vibration response in loess hills due to a high-speed train on railway viaduct," *Research in Cold and Arid Regions*, vol. 14, no. 5, pp. 329–337, 2022.

[31] Y. Shi, "Blasting vibration effect of loess site," *Chinese Journal of Rock Mechanics and Engineering*, vol. 22, no. 11, pp. 1933–1938, 2003.

[32] Y. Shi, L. U. Yu-xia, and H. E. Shao-lin, "Seismic distribution and dynamic stress response characteristics of slope body under blasting vibration," *Chinese Journal of Rock Mechanics and Engineering*, vol. 33, pp. 3707–3717, 2014.

[33] W. Fu, "Distribution rules of collapsible loess and analysis on foundation treatment technology on Baoji-Lanzhou passenger dedicated line," *Railway Standard Design*, vol. 58, no. 11, pp. 15–19, 2014.

[34] K. Xia, L. Dong, X. Pu, and L. I. Lu, "Analysis of seismic response characteristics of loess Tableland," *Rock and Soil Mechanics*, vol. 41, no. 01, pp. 295–304, 2020.

[35] O. Junhiko, *Spectral Analysis of Ground Motion*, Seismology Press, Beijing, China, 2008.